Transcatheter aortic valve replacements alter circulating serum factors to mediate myofibroblast deactivation

Brian A. Aguado[1,2], **Katherine B. Schuetze**[3,4], **Joseph C. Grim**[1,2], **Cierra J. Walker**[2,5], **Anne C. Cox**[1], **Tova L. Ceccato**[2,6], **Aik-Choon Tan**[7], **Carmen C. Sucharov**[3], **Leslie A. Leinwand**[2,6], **Matthew R. G. Taylor**[8], **Timothy A. McKinsey**[3,4,*], **Kristi S. Anseth**[1,2,*]

[1]Department of Chemical and Biological Engineering, University of Colorado Boulder, Boulder, CO 80303, USA

[2]BioFrontiers Institute, University of Colorado Boulder, Boulder, CO 80309, USA

[3]Division of Cardiology, Department of Medicine, University of Colorado Anschutz Medical Campus, Aurora, CO 80045, USA

[4]Consortium for Fibrosis Research and Translation, University of Colorado Anschutz Medical Campus, Aurora, CO 80045, USA

[5]Materials Science and Engineering Program, University of Colorado Boulder, Boulder, CO 80309, USA

[6]Department of Molecular, Cellular, and Developmental Biology, University of Colorado Boulder, Boulder, CO 80309, USA

[7]Department of Biostatistics and Informatics, Colorado School of Public Health, Aurora, CO 80045, USA

[8]Department of Medicine, Adult Clinical Genetics, University of Colorado Health Science Center, Aurora, CO 80045, USA

Abstract

The transcatheter aortic valve replacement (TAVR) procedure has emerged as a minimally invasive treatment for patients with aortic valve stenosis (AVS). However, alterations in serum factor composition and biological activity after TAVR remain unknown. Here, we quantified the systemic inflammatory effects of the TAVR procedure and hypothesized that alterations in serum factor composition would modulate valve and cardiac fibrosis. Serum samples were obtained from patients with AVS immediately before their TAVR procedure (pre-TAVR) and about 1 month afterward (post-TAVR). Aptamer-based proteomic profiling revealed alterations in post-TAVR serum composition, and ontological analysis identified inflammatory macrophage factors implicated in myofibroblast activation and deactivation. Hydrogel biomaterials used as valve matrix mimics demonstrated that post-TAVR serum reduced myofibroblast activation of valvular interstitial cells relative to pre-TAVR serum from the same patient. Transcriptomics and curated network analysis revealed a shift in myofibroblast phenotype from pre-TAVR to post-TAVR and identified p38 MAPK signaling as one pathway involved in pre-TAVR–mediated myofibroblast activation. Post-TAVR serum deactivated valve and cardiac myofibroblasts initially exposed to pre-TAVR serum to a quiescent fibroblast phenotype. Our in vitro deactivation data correlated with patient disease severity measured via echocardiography and multimorbidity scores, and correlations were dependent on hydrogel stiffness. Sex differences in cellular responses to male and female sera were also observed and may corroborate clinical observations regarding sex-specific TAVR outcomes. Together, alterations in serum composition after TAVR may lead to an antifibrotic fibroblast phenotype, which suggests earlier interventions may be beneficial for patients with advanced AVS to prevent further disease progression.

One-sentence summary:

Transcatheter aortic valve replacement alters a patient's serum proteome, reversing valvular interstitial cell and cardiac myofibroblast activation.

Editor's Summary: Responding to replacement

Aortic valve stenosis (narrowing of the aortic valve) contributes to inadequate blood flow, fibrosis, hypertrophy, and, ultimately, heart failure. Transcatheter aortic valve replacement (TAVR) improves blood flow, but little is known about cardiac remodeling after the procedure. Aguado and colleagues performed proteomics on serum samples collected from patients before and after TAVR and studied the effects of serum on valve and cardiac cells using hydrogel culture platforms. A role for p38 MAPK signaling in activating cells was identified using pre-TAVR serum, whereas post-TAVR serum returned cells to a quiescent state. Along with preliminary insights into sex-specific differences, the authors' research supports a role for TAVR-induced alteration of circulating inflammatory cytokines in regulating valve cell phenotype.

INTRODUCTION

Severe aortic valve stenosis (AVS) is a progressive disease characterized by aberrant fibrosis and/or calcification of aortic valve leaflets, leading to inadequate blood flow (1). AVS affects more than the aortic valve; patients also experience increased cardiac hypertrophy and fibrosis during disease progression, which eventually leads to heart failure (2–4). The prevalence of degenerative AVS increases with patient age, affecting 12.4% of the

population over 75 years old, and is considered severe in 3.4% of patients (3). Unfortunately, over 50% of patients succumb to severe AVS 2 years after diagnosis if the disease remains untreated (5). Currently, surgical or transcatheter aortic valve replacements (SAVR or TAVR) serve as the gold standard of treatment for AVS, where a biomaterial-based artificial valve is implanted at the aortic valve site to restore efficient blood flow (6–8). The transfemoral and transapical TAVR procedures were approved for patient use by the Food and Drug Administration in 2011 and 2012, respectively, as less-invasive alternatives to SAVR for high-risk and/or elderly patients (9). Randomized clinical trials suggest that patients receiving TAVR show comparable survival rate outcomes to patients receiving SAVR and that TAVR reverses left ventricular hypertrophy and fibrosis in high-risk surgical patients (9, 10). Hence, there is a need to improve our understanding of how fibrotic tissue remodels after a TAVR procedure and how patient-specific responses to a valve implant may dictate TAVR outcomes.

One hallmark and key mediator of AVS progression is the chronic activation of tissue-specific fibroblasts to myofibroblasts, which are known to cause aberrant tissue stiffening and subsequent fibrosis upon repeated tissue injury (11). Valvular interstitial cells (VICs) activate to myofibroblasts to maintain tissue homeostasis during routine valve injury but remain persistently activated during AVS progression, accompanied by pathological stiffening of the valve leaflets (11). Likewise, patients with AVS experience increased hemodynamic and mechanical stresses during disease progression, subsequently driving increased myofibroblast activation in cardiac tissues (12). After a TAVR procedure, hemodynamic and mechanical stresses on the valve and cardiac tissues are substantially reduced, which can improve left ventricle (LV) function and reduce myofibroblast activation and/or promote myofibroblast deactivation in subsets of patients with AVS (13). Although reductions in mechanical stress likely account for partial reductions or reversal in myofibroblast activity, additional biological mechanisms may also be involved in regulating observed reductions in myofibroblast activation after a TAVR procedure.

Here, serum from patients with AVS was collected before and after a TAVR procedure to elucidate changes in key biological signals that may regulate myofibroblast phenotype after surgery. Postprocedural inflammation has been hypothesized to play a role in mediating TAVR patient outcomes (14). We posit that the systemic inflammatory response to the valve implant and subsequent release of inflammatory cytokines in patient serum may influence fibrotic valve tissue remodeling via regulation of myofibroblasts. We hypothesized that the combination of inflammatory factors in patient serum before TAVR would activate VICs and cardiac fibroblasts to a myofibroblast state, whereas serum factors after TAVR would participate in reversing myofibroblast activation. To test this hypothesis, we characterized the proteome of patient serum samples before and after a TAVR procedure to quantify the global alterations in serum composition and ontologically identified candidate inflammatory factors that may mediate myofibroblast activation [bone morphogenic protein 6 (BMP-6), chemokine C-X-C motif 9 (CXCL9), and interferon-γ (IFN-γ)] and deactivation [tumor necrosis factor–α (TNF-α) and interleukin-1β (IL-1β)]. We used patient sera to treat VICs and adult rat ventricular fibroblasts (ARVFs) cultured on hydrogels that mimic the valve and cardiac extracellular matrix (ECM) to assess myofibroblast activation as a function of serum factors. Quantifying the dynamic alterations in the composition of inflammatory cytokines

after a TAVR procedure may provide insight into the role of circulating serum factors on the fibroblast-to-myofibroblast transition and potential signals that reverse the pathogenic myofibroblast phenotype in patients with AVS.

RESULTS

Pre-TAVR serum activates fibroblasts, whereas post-TAVR serum maintains quiescence

We hypothesized that circulating serum factors in patients with AVS would be altered in response to a TAVR procedure due to the inflammatory response to the implant, which would subsequently affect myofibroblast phenotypes (15). Serum samples were collected from patients immediately before and about 1 month after their TAVR procedure (table S1 in data file S1). Proteomic characterization of patient sera was performed using a SOMAscan DNA aptamer array, where the relative abundances of 1317 proteins were quantified. After comparing the log_2-transformed relative fluorescence unit (RFU) values representing protein abundance before and after the TAVR procedure, we identified 283 differentially regulated proteins [false discovery rate (FDR)–adjusted $P < 0.05$; table S2 in data file S1]. A total of 156 proteins were more abundant in pre-TAVR serum, and 127 proteins were more abundant in post-TAVR serum. Unsupervised hierarchical clustering of differentially expressed serum proteins, based on correlation distance and average linkage, revealed clustering of protein composition for 8 of 12 pre-TAVR and 8 of 12 post-TAVR serum samples (Fig. 1A). SOMAscan data were subsequently analyzed using a scaled principal component analysis (PCA) to visualize variation between serum samples before and after a TAVR procedure. Principal component (PC) 1 (45.3%) differentiated pre-TAVR and post-TAVR samples into clustered groups, suggesting a shift in serum protein composition after a TAVR procedure (Fig. 1B).

Next, we queried whether factors present in pre-TAVR and post-TAVR sera would affect myofibroblast activation in vitro. Myofibroblast activation was quantified as the percentage of cells containing α-smooth muscle actin (α-SMA) stress fibers in an immunofluorescence image. Aortic VICs seeded on tissue culture polystyrene (TCPS) treated with serum from patients before and after TAVR showed no significant differences in myofibroblast activation, although serum from patients A, B, C, D, and E showed trends toward decreased activation in post-TAVR serum (fig. S1). Recognizing that TCPS causes rampant myofibroblast activation, in part due to its supraphysiologic stiffness, we next identified hydrogel formulations (16) that would promote VIC attachment, with moduli that more closely match the mechanical microenvironments associated with cells in the valve. Synthetic poly(ethylene glycol) (PEG) hydrogels were generated using photoinitiated thiol-ene click chemistry (17) to create defined microenvironments that mimic the mechanical properties of valvular tissue (Fig. 1C). By altering the final PEG polymer weight percent (4 and 10%), soft and stiff hydrogel scaffolds were generated with elastic moduli (E) of 5.8 and 40.4 kPa, which correspond to healthy and fibrotic valve leaflet stiffness, respectively (fig. S2) (18). Hydrogel stiffness could be tuned to regulate VIC myofibroblast phenotype, where stiffer hydrogels (intended to mimic fibrotic valve tissue) activated VICs to a myofibroblast state and the baseline soft formulation allowed long-term culture of quiescent VIC fibroblasts (19, 20).

We used the soft PEG hydrogel formulations as a substrate to probe the effects of pre-TAVR and post-TAVR sera on the VIC fibroblast phenotype. We confirmed that VICs retained a quiescent fibroblast-like phenotype on soft hydrogels in the presence of both fetal bovine serum (FBS) (31.3 ± 9.5%) and human serum from a healthy male patient (28.1 ± 10.8%), whereas they activated to myofibroblasts (62.3 ± 7.1%) in the presence of transforming growth factor–β1 (TGF-β1) (fig. S3) (21). Using these parameters as negative and positive controls for myofibroblast activation, respectively, we hypothesized that serum from a patient obtained before a TAVR procedure would promote a myofibroblast phenotype, whereas serum from the same patient obtained after a TAVR procedure would maintain fibroblast quiescence (Fig. 1D). Consistent with our hypothesis, we observed that pre-TAVR serum activated VICs to a myofibroblast state, and post-TAVR serum maintained fibroblast quiescence (Fig. 1E). VICs treated with pre-TAVR sera from six of eight patients had elevated percentages of activated myofibroblasts relative to post-TAVR serum treatments from the same patient (Fig. 1F). After normalizing the quantified post-TAVR activation percentages to the average pre-TAVR activation percentage, we observed patient-specific differences in the fold change reductions of myofibroblast activation in the presence of post-TAVR serum factors (Fig. 1G).

The phenotypic shifts in myofibroblast activation observed as a function of serum treatment led us to hypothesize that specific serum factors may be mediating activation and quiescence in pre-TAVR and post-TAVR sera, respectively. We performed an ontological analysis using the Database for Annotation, Visualization, and Integrated Discovery (DAVID version 6.8) to identify enriched gene ontology (GO) functions, including biological processes, molecular functions, and cellular components categories for proteins up-regulated in pre-TAVR (table S3 in data file S1) and post-TAVR (table S4 in data file S1) sera. After categorizing proteins associated with the immune response, extracellular space, and cytokine signaling, we narrowed down our list of candidate factors that may mediate fibrotic tissue remodeling. In pre-TAVR serum, we identified 15 candidate factors that promote a fibrotic phenotype (Fig. 1H). Using the same strategy, we identified 14 candidate factors in post-TAVR serum that likely promote reverse remodeling of fibrotic tissue (Fig. 1I).

VIC transcriptome reveals pathways regulating myofibroblast phenotype in TAVR serum

Next, we sought to identify critical signaling pathways involved in serum-mediated myofibroblast activation. Using next-generation RNA sequencing techniques to characterize the transcriptome of VICs treated with pre-TAVR and post-TAVR sera, we hypothesized that key signaling pathways would emerge as potential regulators of serum-mediated myofibroblast activation. After comparing the counts per million read values for all samples (n = 8 pre-TAVR patients and n = 8 post-TAVR patients), 1193 genes were differentially expressed in VICs treated with pre-TAVR serum relative to post-TAVR serum (FDR-adjusted P value cutoff of 0.05; table S5 in data file S1). A mean-difference (MD) plot depicted the 619 up-regulated and 574 down-regulated genes in pre-TAVR serum, as well as the genes with expression changes greater than 1.0 or less than −1.0 log-twofold change relative to post-TAVR samples (Fig. 2A). From the differentially regulated gene list, we curated genes specific to cytoskeletal organization (nine up and two down), ECM remodeling (seven up and six down), and fibrocalcification (five up and three down)

processes (Fig. 2B), which revealed a myofibroblast phenotypic shift from pre-TAVR to post-TAVR (Fig. 2C).

Next, we cataloged the most relevant pathways up- and down-regulated in response to patient serum samples using the Kyoto Encyclopedia of Genes and Genomes (KEGG) database. For up-regulated genes, the mitogen-activated protein kinase (MAPK) pathway, Hippo pathway, and pathways associated with focal adhesion were enriched and top ranked according to the gene ratio of up-regulated genes to the total number of genes in the pathway (table S6 in data file S1 and Fig. 2D). Pathways associated with infection, proteoglycan signaling, and protein processing in the endoplasmic reticulum were enriched and top ranked according to the gene ratio for down-regulated genes (table S7 in data file S1 and Fig. 2E). Next, we identified upstream regulators of myofibroblast activation present in pre-TAVR serum that act on the MAPK signaling pathway. We generated interaction networks with our list of differentially regulated genes in pre-TAVR serum using the Ingenuity Pathway Analysis (IPA) and added the 15 candidate factors regulating myofibroblast activation in pre-TAVR serum (Fig. 1H) to the top-ranked curated interaction network. Expanding the network by one interaction to include our 15 candidate factors as nodes showed 7 of 15 factors connected to the network generated using IPA, which serve as upstream regulators of p38 MAPK (Fig. 2F).

Individual factors in pre-TAVR serum activate VICs on hydrogel valve–ECM mimics

To validate candidate factors as inducers of myofibroblast activation, we used physiologically relevant hydrogel microenvironments that allow culture of quiescent VIC fibroblasts. We evaluated the role of IFN-γ, BMP-6, and CXCL9, three of the seven candidate factors identified as upstream regulators of MAPK signaling from our IPA analysis (Fig. 2F). We observed increased myofibroblast activation as a function of IFN-γ, BMP-6, and CXCL9 concentrations in VICs seeded on soft hydrogels (fig. S4).

Next, we evaluated the ability of post-TAVR serum to deactivate VICs initially activated with BMP-6, CXCL9, or IFN-γ and assessed variability in deactivation as a function of patient sera. During a 5-day study, VICs were seeded on soft hydrogels, treated with 100 ng/ml of IFN-γ, BMP-6, or CXCL9, and then treated with control or post-TAVR serum from four patients (Fig. 3A). VICs activated to a myofibroblast state when treated with BMP-6, despite removing BMP-6 in exchange for control medium, whereas post-TAVR serum deactivated VICs (Fig. 3B). BMP-6–activated VICs deactivated in the presence of post-TAVR serum (four of four patient sera tested) (Fig. 3C), with patient-specific differences in the extent of deactivation (Fig. 3D). Similarly, CXCL9 activated VICs to a myofibroblast state, whereas post-TAVR serum deactivated cells (Fig. 3E). CXCL9-activated VICs returned to a quiescent state in the presence of post-TAVR serum from all four patient sera tested (Fig. 3F), with patient-specific differences in deactivation (Fig. 3G). In contrast, IFN-γ did not maintain VIC activation upon removal of the cue (Fig. 3H). Using post-TAVR serum treatments, only one of four patients' sera reduced VIC activation after IFN-γ treatment (Fig. 3I), although we did observe patient-specific differences in deactivation as previously observed with BMP-6 and CXCL9 (Fig. 3J). Together, our data suggest that post-

TAVR serum contains factors that deactivate myofibroblasts initially treated with candidate factors identified in pre-TAVR serum.

Pre-TAVR serum regulates myofibroblast activation via MAPK signaling

The convergence of our proteomic and transcriptomic results on MAPK signaling as a candidate pathway mediating myofibroblast activation in pre-TAVR serum suggested that we validate the potential role of p38 MAPK in mediating downstream α-SMA stress fiber formation. We first confirmed VICs had reduced α-SMA stress fiber formation, even in the highly activating TCPS microenvironment, in the presence of SB203580, a small-molecule inhibitor of p38 MAPK activity (fig. S5). Using SB203580 to inhibit p38 MAPK activity in VICs seeded on soft hydrogels, we observed that p38 MAPK–inhibited VICs had decreased myofibroblast activation in response to pre-TAVR serum from four patients (selected because of serum availability) (Fig. 4A). For three of four serum samples tested, we observed decreased α-SMA stress fiber formation in VICs treated with 20 μM SB203580 relative to vehicle controls (Fig. 4B). We also observed decreased myofibroblast activation using SB203580 in the presence of individual cytokines (Fig. 4C). Specifically, treatment with 20 μM SB203580 reduced myofibroblast activation in the presence of BMP-6 and CXCL9 relative to vehicle controls (Fig. 4D).

Post-TAVR serum reverses valvular myofibroblast activation on soft and stiff hydrogels

Next, we tested the ability of post-TAVR serum to reverse the activated myofibroblast phenotype using our controlled in vitro hydrogel model. VICs are rampantly activated toward a myofibroblast state on TCPS, and we did not observe any deactivation of TCPS-cultured VICs in the presence of post-TAVR serum (fig. S6). VICs activated to a myofibroblast state using pre-TAVR serum for 48 hours were then treated with either pre-TAVR or post-TAVR serum from the same patient (Fig. 5A). In the soft hydrogel microenvironments, we observed deactivation, or reversal of the pre-TAVR–mediated activation of VICs, by exposure to post-TAVR patient serum (Fig. 5B). For six of eight patients, VICs remained highly activated in pre-TAVR serum, but the activation was reversed in the presence of post-TAVR serum (Fig. 5C). We also observed differences in the fold change deactivation of myofibroblasts between patients (Fig. 5D). There was no significant correlation between the fold change deactivation values for each patient according to aortic valve area values measured using echocardiography (Fig. 5E).

To determine whether VIC activation was context specific, we tested whether myofibroblasts would revert to a fibroblast (quiescent) phenotype in response to serum cues if the microenvironment was stiffer, similar to that of diseased, fibrotic valve tissue. First, we confirmed the percentage of activated myofibroblasts was greater on stiff ($55.5 \pm 10.5\%$) relative to soft ($37.0 \pm 11.0\%$) hydrogels (fig. S7). Post-TAVR serum deactivated myofibroblasts on stiff hydrogels (Fig. 5F). VICs treated with pre-TAVR serum remained highly activated on stiff hydrogels, but the myofibroblast population decreased in the presence of post-TAVR serum from six of eight patients (Fig. 5G). Patient-specific differences in post-TAVR serum–mediated deactivation were also apparent on stiff hydrogels (Fig. 5H). We observed a significant negative correlation between fold change deactivation values and aortic valve area measured by echocardiography, suggesting a link between in

vitro myofibroblast deactivation on stiff hydrogels and valve area, where decreased valve area serves as an indicator of AVS disease severity (Fig. 5I).

Post-TAVR serum reverses cardiac myofibroblast activation on soft and stiff hydrogels

Given clinical data suggesting fibrotic left ventricular tissue remodels after TAVR, we investigated how post-TAVR serum factors deactivate cardiac myofibroblasts. LV ARVFs were seeded on soft or stiff hydrogels and treated with pre-TAVR and post-TAVR sera, as described for VICs (Fig. 5A). Fibrotic cardiac tissue is considerably stiffer than fibrotic valvular tissue (22, 23); therefore, we altered our stiff hydrogel formulation to generate 278-kPa hydrogels (fig. S2). We confirmed ARVFs are mechanosensitive, because ARVFs maintained low activation on soft hydrogels in both FBS ($24.0 \pm 6.6\%$) and healthy human serum ($28.6 \pm 21.4\%$) but increased activation on stiff hydrogels (FBS, $61.7 \pm 8.1\%$; healthy human serum, $60.1 \pm 16.8\%$) (fig. S8).

Pre-TAVR serum activated ARVFs seeded on soft hydrogels to differentiate into myofibroblasts, and a subsequent post-TAVR serum treatment deactivated the cells (Fig. 6A). For five of eight patients, ARVFs activated in pre-TAVR serum and deactivated when treated with post-TAVR serum (Fig. 6B). Patient-specific deactivation fold changes were observed (Fig. 6C), which correlated with deactivation fold changes observed in VICs (fig. S9). Cardiac myofibroblasts showed high activation in pre-TAVR serum on stiff hydrogels, and activation was significantly reduced in post-TAVR serum (Fig. 6D). For seven of eight patients, ARVFs were activated by pre-TAVR serum and deactivated upon treatment with post-TAVR serum (Fig. 6E), showing patient-specific deactivation (Fig. 6F).

Fold change deactivation values of ARVFs treated with individual patient sera on soft hydrogels did not correlate with Society of Thoracic Surgery (STS) risk scores of patient mortality after TAVR (Fig. 6G); however, STS scores correlated with patient-specific serum deactivation values on stiff hydrogels (Fig. 6H). Similarly, ARVF deactivation data on soft hydrogels did not correlate with left ventricular internal diameter measurements in both systole (LVIDs; Fig. 6I) and diastole (LVIDd; Fig. 6J), whereas stiff hydrogel ARVF deactivation data negatively correlated with LVIDs (Fig. 6K) and LVIDd (Fig. 6L) measurements. Thus, ARVFs that were less reversible in vitro corresponded to more severely diseased patients with reduced LV diameters due to wall thickening.

Validating inflammatory factors mediating myofibroblast deactivation using stiff hydrogels

Given the complex milieu of factors present in post-TAVR serum that override mechanical signals from the matrix environment, we next sought to validate key serum proteins as mediators of the observed myofibroblast deactivation. On the basis of our SOMAscan results, we selected the inflammatory cytokines IL-1β and TNF-α, which were both more abundant in post-TAVR serum relative to pre-TAVR serum. We hypothesized that TNF-α and IL-1β would deactivate myofibroblasts on stiff hydrogels, and subsequently observed decreases in myofibroblast activation as a function of cytokine concentration (fig. S10). VICs cultured on stiff hydrogels treated with pre-TAVR serum remained activated when subsequently treated with control media, whereas activated cells subsequently treated with IL-1β and TNF-α (10 ng/ml) deactivated, with reduced α-SMA stress fiber formation (Fig.

7, A and B). For three of four serum samples tested, IL-1β and TNF-α deactivated pre-TAVR–activated VICs (Fig. 7C). Patient-specific differences were observed in the deactivation fold changes (Fig. 7, D and E).

Next, we queried the role of inflammatory cytokines released from M1 proinflammatory macrophages in deactivating VICs. THP-1 monocytes were differentiated into M1 macrophages and used to generate conditioned media for VIC culture. As hypothesized, conditioned medium from M1 macrophages deactivated VICs seeded on stiff hydrogels in a concentration-dependent manner (Fig. 7, F and G). Enzyme-linked immunosorbent assay (ELISA) confirmed that conditioned medium from M1 macrophages contained increased TNF-α (562.7 ± 68.5 pg/ml) and IL-1β (207.1 ± 12.3 pg/ml) relative to control medium (Fig. 7H), further suggesting these M1 macrophage factors are involved in deactivating myofibroblasts.

Sex-specific differences in serum-mediated activation and deactivation

Recognizing that male and female patients experience different outcomes in fibrotic tissue remodeling after TAVR (24, 25), we reanalyzed our VIC activation and deactivation data, looking for differences in responses to serum from male and female patients. We observed that five of eight pre-TAVR samples and six of eight post-TAVR samples from male patients clustered together and three of four post-TAVR serum samples from female patients clustered together (fig. S11). Pooling the quantified myofibroblast activation results according to the sex of the patient demonstrated that 26.5 ± 9.8% of VICs treated with post-TAVR serum from male patients were activated to myofibroblasts, lower than 37.4 ± 8.4% of VICs treated with post-TAVR serum from female patients (Fig. 8A). The fold change in VIC activation was reduced in male serum relative to female serum (Fig. 8B). Upon reanalyzing our pre-TAVR versus post-TAVR proteomic results and separating by sex ($n = 8$ male patients and $n = 4$ female patients), we observed a total of 39 proteins with abundance changes in female serum, whereas we observed 347 proteins to have altered abundances in male serum, with 88 differentially regulated proteins in common between sexes (Fig. 8C). IL-1β and TNF-α were more abundant in male post-TAVR serum relative to pre-TAVR serum; BMP-6 was more abundant in male pre-TAVR serum relative to post-TAVR; and CXCL9 and IFN-γ were more abundant in both male and female pre-TAVR serum relative to post-TAVR serum (table S8 in data file S1). Reanalyzing our transcriptomics data ($n = 4$ male patients and $n = 4$ female patients) revealed a total of 23 genes in VICs were differentially regulated when treated with female serum, whereas 452 genes were differentially regulated when treated with male serum, with 35 differentially regulated genes in common between male and female serum-treated VICs (Fig. 8D and table S9 in data file S1).

We also observed sex-specific differences in our deactivation experiments on hydrogel substrates. On soft hydrogels, VICs treated with male pre-TAVR serum for the entire experiment had higher activation relative to female pre-TAVR serum treatments, and VICs deactivated with post-TAVR serum showed less deactivation in male serum relative to female serum (Fig. 8, E and F). Similar trends were observed in ARVFs, where male and female post-TAVR serum deactivated myofibroblasts on soft substrates, with less

deactivation in male serum relative to female serum (Fig. 8, G and H). Because we demonstrated that deactivation fold changes on stiff hydrogels correlated with patient data, we next analyzed sex differences in deactivation on stiff hydrogels. VICs treated with serum from male and female patients activated in pre-TAVR and deactivated in post-TAVR similarly (Fig. 8I), with no change in fold change deactivation (Fig. 8J). However, ARVFs treated with male post-TAVR serum showed greater deactivation relative to ARVFs treated with female serum (Fig. 8K), with a reduction in fold change activation levels (Fig. 8L).

DISCUSSION

Here, we quantified the differences in circulating factor composition in patient sera after a TAVR procedure, identifying factors that promote valvular and cardiac myofibroblast deactivation. We suggest inflammatory macrophages arriving to valve implants partially contribute to altering secreted factors in the blood and promote an antifibrotic phenotype to assist left ventricular reverse remodeling (24). Prior studies of transcatheter aortic valves suggest proinflammatory immune cells accumulate along the artificial valve leaflet, indicating immune cells arrive and adhere to the implant (26). Although other contributors, including activation of the renin-angiotensin system (27) and reduction in sympathetic activity after TAVR (28), can lead to systemic alterations in serum factors, our data suggest that the systemic inflammation response to the TAVR implant is involved in altering the composition of patient serum factors, at least when measured at an acute 30-day time point. Our SOMAscan proteomic (29) and GO analysis strategy shows enrichment of dozens of proteins associated with the inflammation response after TAVR, particularly proteins traditionally secreted by inflammatory macrophages, including TNF-α and IL-1β. TNF-α and IL-1β secreted from proinflammatory macrophages were shown to deactivate myofibroblasts on stiff hydrogels, supporting the premise that inflammatory proteins partially regulate myofibroblast deactivation after a TAVR procedure.

The role of TNF-α and IL-1β in mediating myofibroblast phenotypes has been controversial (30, 31). TNF-α has been previously shown to reduce α-SMA expression in myofibroblasts (32), reduce collagen production via nuclear factor κB signaling (33), inhibit TGF-β myofibroblast signaling (34), and have increased abundance in serum after TAVR and SAVR (14, 35). Likewise, IL-1β has been shown to mitigate TGF-β1–mediated cardiac myofibroblast activation (36). In contrast, other studies suggest TNF-α secretion from inflammatory macrophages promotes osteogenic differentiation of VICs (37–40). In addition, IL-1 receptor antagonist knockout mice spontaneously develop AVS, which implicates IL-1β in promoting calcification (41). Considering our in vitro results, we posit that the effects of TNF-α and IL-1β after TAVR are tissue specific. In valvular tissue, VICs likely adopt an antifibrotic and procalcific phenotype in response to TNF-α and IL-1β during AVS progression. After a TAVR procedure, elevated TNF-α and IL-1β secreted from proinflammatory macrophages would contribute to modifying the valve tissue microenvironment, potentially influencing bioprosthetic and native valve restenosis and other structural deteriorations around the annulus in the long term (14, 42, 43). In cardiac tissue, TNF-α and IL-1β likely participate in deactivating myofibroblasts in left ventricular tissue, because previous work has shown these factors decrease collagen production and increase MMP activity (44). Open questions remain regarding the effects of TNF-α and

IL-1β (and potentially other post-TAVR factors) in mediating osteogenic VIC differentiation and subsequent valve restenosis given their procalcific effects, even though these factors may provide antifibrotic benefits to diseased cardiac tissue. Collectively, evidence supports the notion that serum factors (such as TNF-α, IL-1β, and other post-TAVR factors) may play a critical role in myofibroblast deactivation after TAVR, which could further affect valvular and cardiac fibrosis and potentially be used as markers to monitor a patient's beneficial response to TAVR.

The use of soft hydrogel culture platforms enabled the unambiguous assessment of inflammatory factors on the fibroblast-to-myofibroblast transition by decoupling mechanically induced myofibroblast activation. Because TCPS automatically activates fibroblasts to myofibroblasts, hydrogel culture platforms are an essential tool for studying valvular and cardiac fibroblast phenotypes and myofibroblast activation in vitro (18, 21, 45–48). Our results on soft hydrogels implicate serum factors in patients with AVS as drivers of myofibroblast activation in valvular and cardiac tissue relative to healthy serum controls, suggesting serum factors exacerbate tissue fibrosis during AVS. Merging high-throughput datasets (49–51) yielded candidate proteins in the pre-TAVR serum milieu that may serve to promote myofibroblast activation via the p38 MAPK pathway. Signaling via p38 MAPK has been implicated in driving myofibroblast activation during fibrosis progression in different tissues (52–55). Proteins upstream of the MAPK pathway according to our IPA analysis, including IFN-γ, BMP-6, and CXCL9, were validated as candidate factors mediating myofibroblast activation, thus implicating these factors in partially contributing to AVS progression (56, 57). Future work comparing concentrations of IFN-γ, BMP-6, and CXCL9 in patients with AVS relative to healthy patients may further implicate these factors as biomarkers and contributors to AVS progression. Together, our soft hydrogel system serves as a critical tool for maintaining fibroblast quiescence to probe the roles of serum factors and signaling pathways that may drive myofibroblast activation and subsequent AVS progression.

Post-TAVR serum also deactivates valvular and cardiac myofibroblasts on stiff, fibrotic-like microenvironments, and the fold change in deactivation correlates with measures of patient disease severity (smaller aortic valve area, higher STS score, and lower LVIDs/LVIDd measurements). We suggest that our engineered hydrogels can serve as in vitro models to support precision medicine and serve as precision biomaterials that enable patient-specific evaluation of disease (58). As an example, previous clinical work suggests LV reverse remodeling is predictive of improved survival outcomes after TAVR, where patients lacking LV reverse remodeling were observed to die within the first year after TAVR (13). Given that improvements in LV remodeling correlate with TAVR outcomes and serum factors after TAVR mediate myofibroblast deactivation in fibrotic microenvironments, we posit that earlier TAVR procedures may prove beneficial for patients with AVS to prevent further fibrosis progression and promote tissue remodeling. Because valve and cardiac fibrosis are difficult to treat and no known drugs exist to reverse or slow disease progression (59), we also envision an opportunity to develop in vitro models that more accurately reflect in vivo disease context to identify new pathways for drugs to target fibrosis. Although our results reveal the potential impact of this strategy, future work is needed to fully evaluate our in vitro correlations with patient data, especially studies that include larger sample sizes,

tracking patient sera with time, and/or using human-derived fibroblast populations. Given prior reports suggesting cardiac tissue remodeling occurs over months after aortic valve replacement (24), evaluating the longitudinal effects of post-TAVR serum factors in patients (at least 6 months) may further reveal the potential role of serum factors in mediating long-term fibrotic tissue remodeling. However, the reported results support the role of engineered biomaterials and in vitro models to advance the understanding of disease context in vivo; this complementary integration of in vitro and in vivo studies should prove beneficial for considering earlier TAVR procedures to improve patient outcomes.

Sex-specific AVS progression (60–62) and TAVR outcomes (63, 64) have also been observed, suggesting an opportunity to identify sex differences in how serum factors altered after a TAVR procedure may mediate resolution of fibrotic valvular and cardiac tissue. Our sex-separated pre-TAVR versus post-TAVR characterization of myofibroblast activation on soft hydrogels revealed VICs treated with male post-TAVR serum have reduced myofibroblast activation relative to female post-TAVR sera, possibly due to the increased abundance of TNF-α and IL-1β in male sera after TAVR. In addition, VICs preexposed to male pre-TAVR serum have reduced ability to deactivate in male post-TAVR serum on soft hydrogels relative to female sera. We suggest that male pre-TAVR serum factors likely prime VICs toward cellular phenotypes that promote calcification. Ultimately, this reduces their ability to deactivate after TAVR and is consistent with clinical observations that men have worse comorbidities, increased reintervention risks, and reduced survival rates due to increased fibro-calcification at the valve relative to women (63, 64). Further, in the LV, female ventricular tissue is predominantly hypertrophic with reduced interstitial fibrosis compared with male patients (65, 66), which is consistent with our observation that ARVFs treated with female sera have improved deactivation relative to male sera treatments on soft hydrogels. The factors leading to these sex differences are likely multivariate, including differences in renin-angiotensin activation, postmenopausal estrogen concentrations, nitric oxide levels, and circulating noradrenaline (among other factors) in female serum (67). However, our ARVF deactivation results, where male sera showed more pronounced ARVF deactivation relative to female sera on stiff hydrogels, seem to corroborate the clinical observation that males experience superior reverse LV remodeling relative to women due to increased initial adverse remodeling before TAVR (24). Our results suggest that this may be due to more abundant TNF-α and IL-1β in male sera, and because LV reverse remodeling is beneficial for TAVR patients, these results further motivate future investigations into earlier TAVR placements for patients with AVS, particularly men. Together, we propose that the sex differences observed in this study are context specific, namely, requiring appropriate biomaterial culture systems, because they depend on synergies between in vitro biomechanical and biochemical cues. Although future work is required to fully dissect the sex-specific mechanisms guiding VIC and ARVF deactivation after TAVR, our work demonstrates the importance of considering sex as a biological variable not only in clinical data but also in in vitro experimentation.

In summary, proteomic analysis of patient sera demonstrates that TAVR procedures, as well as the introduction of a biomaterial device into the heart, alter circulating protein composition in a beneficial way that can reverse myofibroblast activation in fibrotic valve and cardiac tissues. This was confirmed by in vitro experiments that enabled a systematic

evaluation of the effects of patient-specific serum factors on VICs and ARVFs and their myofibroblast activation and deactivation. Specifically, hydrogel culture systems that recapitulate soft tissue, as well as fibrotic microenvironments, were used to generate in vitro models of heart disease to provide a bridge to better understand disease progression and resolution after TAVR in vivo. Of course, the complex interplay between extracellular biochemical and mechanical cues regulating valvular and cardiac fibrosis will certainly require further investigation. Because the field seeks to identify drugs and treatments to reduce detrimental, persistent myofibroblast activation in fibrotic tissues, model systems that allow researchers to elucidate the effects of differential and synergistic micro-environmental factors will become increasingly important. Collectively, we suggest engineered biomaterial in vitro culture systems coupled with biochemical cues from sera provide a more clinically relevant in vitro model for understanding disease context in vivo, which may lead to identifying patient-specific mechanisms of AVS progression and pathways to customized treatments and earlier interventions.

MATERIALS AND METHODS

Study design

We hypothesized serum factors before a TAVR procedure would activate valvular and cardiac fibroblasts to myofibroblasts, whereas serum factors after a TAVR procedure would lead to their deactivation. Patient serum was collected under approval from the Colorado Multiple Institutional Review Board (IRB) (CO-MIRB 07–0516). All patients completed an IRB-approved informed consent form. All samples for research purposes have been deidentified. Patients were seen in a multidisciplinary valve clinic where they were evaluated by a cardiac surgeon and interventional cardiologist. The patients were all deemed either high or intermediate risk for SAVR. All patients received the Sapien 3 (Edwards Lifesciences) balloon expandable transcatheter heart valve via femoral artery access. Blood samples were obtained at the time of access for TAVR and at the one month outpatient follow up visit. All patients underwent equivalent treatment protocols before and after surgery. A total of $n = 12$ pre-TAVR serum samples and $n = 12$ post-TAVR serum samples were collected (table S1 in data file S1) for proteomic characterization using a SOMAscan DNA aptamer array (SomaLogic) according to the manufacturer's protocol and previous studies (29, 68). Serum samples were also used to treat porcine VICs and ARVFs seeded on PEG hydrogels to characterize the effects of serum factors on myofibroblast activation and deactivation. Animal studies were performed in accordance with institutional guidelines and protocols approved by the University of Colorado Boulder Institutional Animal Care and Use Committee. Healthy serum samples were also used for in vitro experimentation from one male and one female patient for control experiments (both patients 60 years in age). The minimum sample size for all experiments was calculated using a type I error rate of 0.05 and power of 0.8 in detecting differences in means of at least 30%. Researchers performing in vitro work were blinded to clinical data until results were obtained to perform correlation analyses. Detailed methods on the SOMAscan array, PEG-norbornene synthesis, hydrogel fabrication, rheological characterization, VIC/ARVF/macrophage cell culture, myofibroblast characterization, M1 macrophage conditioned media generation, RNA library preparation,

transcriptome analysis pipelines used (69–72), and protein validation studies can be found in the Supplementary Materials and Methods.

Statistical analysis

Data are shown as the means ± SD unless otherwise stated. Significance was claimed at *$P <$ 0.05, **$P <$ 0.01, ***$P <$ 0.001, and ****$P <$ 0.0001 using a one-way or two-way analysis of variance (ANOVA) with Tukey posttests for multiple comparisons in GraphPad Prism unless otherwise stated. Correlations between data were determined using standard linear regression and goodness-of-fit tests in GraphPad Prism. Individual subject-level data are provided in data file S2.

Supplementary Material

Refer to Web version on PubMed Central for supplementary material.

Acknowledgments:

REFERENCES AND NOTES

1. Weiss RM, Miller JD, Heistad DD, Fibrocalcific aortic valve disease: Opportunity to understand disease mechanisms using mouse models. Circ. Res 113, 209–222 (2013). [PubMed: 23833295]

2. Carroll JD, TAVR prognosis, aging, and the second TAVR tsunami: Insights from France. J. Am. Coll. Cardiol 68, 1648–1650 (2016). [PubMed: 27712777]

3. Osnabrugge RLJ, Mylotte D, Head SJ, Van Mieghem NM, Nkomo VT, LeReun CM, Bogers AJJC, Piazza N, Kappetein AP, Aortic stenosis in the elderly: Disease prevalence and number of candidates for transcatheter aortic valve replacement: A meta-analysis and modeling study. J. Am. Coll. Cardiol 62, 1002–1012 (2013). [PubMed: 23727214]

4. Vahl TP, Kodali SK, Leon MB, Transcatheter aortic valve replacement 2016: A modern-day "through the looking-glass" adventure. J. Am. Coll. Cardiol 67, 1472–1487 (2016). [PubMed: 27012409]

5. Otto CM, Prendergast B, Aortic-valve stenosis—From patients at risk to severe valve obstruction. N. Engl. J. Med 371, 744–756 (2014). [PubMed: 25140960]

6. Leon MB, Smith CR, Mack M, Miller DC, Moses JW, Svensson LG, Tuzcu EM, Webb JG, Fontana GP, Makkar RR, Brown DL, Block PC, Guyton RA, Pichard AD, Bavaria JE, Herrmann HC, Douglas PS, Petersen JL, Akin JJ, Anderson WN, Wang D, Pocock S; PARTNER Trial Investigators, Transcatheter aortic-valve implantation for aortic stenosis in patients who cannot undergo surgery. N. Engl. J. Med 363, 1597–1607 (2010). [PubMed: 20961243]

7. Marquis-Gravel G, Redfors B, Leon MB, Généreux P, Medical treatment of aortic stenosis. Circulation 134, 1766–1784 (2016). [PubMed: 27895025]

8. Généreux P, Head SJ, Wood DA, Kodali SK, Williams MR, Paradis J-M, Spaziano M, Kappetein AP, Webb JG, Cribier A, Leon MB, Transcatheter aortic valve implantation 10-year anniversary: Review of current evidence and clinical implications. Eur. Heart J 33, 2388–2398 (2012). [PubMed: 22851654]

9. Smith CR, Leon MB, Mack MJ, Miller DC, Moses JW, Svensson LG, Tuzcu EM, Webb JG, Fontana GP, Makkar RR, Williams M, Dewey T, Kapadia S, Babaliaros V, Thourani VH, Corso P, Pichard AD, Bavaria JE, Herrmann HC, Akin JJ, Anderson WN, Wang D, Pocock SJ; PARTNER Trial Investigators, Transcatheter versus surgical aortic-valve replacement in high-risk patients. N. Engl. J. Med 364, 2187–2198 (2011). [PubMed: 21639811]

10. Reardon MJ, Adams DH, Kleiman NS, Yakubov SJ, Coselli JS, Deeb GM, Gleason TG, Lee JS, Hermiller JB Jr., Chetcuti S, Heiser J, Merhi W, Zorn GL III, Tadros P, Robinson N, Petrossian G, Hughes GC, Harrison JK, Maini B, Mumtaz M, Conte JV, Resar JR, Aharonian V, Pfeffer T, Oh JK, Qiao H, Popma JJ, 2-year outcomes in patients undergoing surgical or self-expanding transcatheter aortic valve replacement. J. Am. Coll. Cardiol 66, 113–121 (2015). [PubMed: 26055947]

11. Wang H, Leinwand LA, Anseth KS, Cardiac valve cells and their microenvironment—Insights from in vitro studies. Nat. Rev. Cardiol 11, 715–727 (2014). [PubMed: 25311230]

12. Ozkan A, Kapadia S, Tuzcu M, Marwick TH, Assessment of left ventricular function in aortic stenosis. Nat. Rev. Cardiol 8, 494–501 (2011). [PubMed: 21670747]

13. Sato K, Kumar A, Jones BM, Mick SL, Krishnaswamy A, Grimm RA, Desai MY, Griffin BP, Rodriguez LL, Kapadia SR, Obuchowski NA, Popovic ZB, Reversibility of cardiac function predicts outcome after transcatheter aortic valve replacement in patients with severe aortic stenosis. J. Am. Heart Assoc 6, e005798 (2017). [PubMed: 28698259]

14. Sulženko J, Toušek P, Ko ka V, Bedná F, Línková H, Petr R, Laboš M, Widimský P, Degenerative changes and immune response after transcatheter aortic valve implantation. Comparison with surgical aortic valve replacement. J. Cardiol 69, 483–488 (2017). [PubMed: 27117541]

15. Erdoes G, Lippuner C, Kocsis I, Schiff M, Stucki M, Carrel T, Windecker S, Eberle B, Stueber F, Book M, Technical approach determines inflammatory response after surgical and transcatheter aortic valve replacement. PLOS ONE 10, e0143089 (2015). [PubMed: 26599610]

16. Mabry KM, Lawrence RL, Anseth KS, Dynamic stiffening of poly(ethylene glycol)-based hydrogels to direct valvular interstitial cell phenotype in a three-dimensional environment. Biomaterials 49, 47–56 (2015). [PubMed: 25725554]

17. Fairbanks BD, Schwartz MP, Halevi AE, Nuttelman CR, Bowman CN, Anseth KS, A versatile synthetic extracellular matrix mimic via thiol-norbornene photopolymerization. Adv. Mater 21, 5005–5010 (2009). [PubMed: 25377720]

18. Kloxin AM, Benton JA, Anseth KS, In situ elasticity modulation with dynamic substrates to direct cell phenotype. Biomaterials 31, 1–8 (2010). [PubMed: 19788947]

19. Wang H, Haeger SM, Kloxin AM, Leinwand LA, Anseth KS, Redirecting valvular myofibroblasts into dormant fibroblasts through light-mediated reduction in substrate modulus. PLOS ONE 7, e39969 (2012). [PubMed: 22808079]

20. Wang H, Tibbitt MW, Langer SJ, Leinwand LA, Anseth KS, Hydrogels preserve native phenotypes of valvular fibroblasts through an elasticity-regulated PI3K/AKT pathway. Proc. Natl. Acad. Sci. U.S.A 110, 19336–19341 (2013). [PubMed: 24218588]

21. Gould ST, Darling NJ, Anseth KS, Small peptide functionalized thiol-ene hydrogels as culture substrates for understanding valvular interstitial cell activation and de novo tissue deposition. Acta Biomater 8, 3201–3209 (2012). [PubMed: 22609448]

22. Berry MF, Engler AJ, Woo YJ, Pirolli TJ, Bish LT, Jayasankar V, Morine KJ, Gardner TJ, Discher DE, Sweeney HL, Mesenchymal stem cell injection after myocardial infarction improves myocardial compliance. Am. J. Physiol. Heart Circ. Physiol 290, H2196–H2203 (2006). [PubMed: 16473959]

23. Hiesinger W, Brukman MJ, McCormick RC, Fitzpatrick JR III, Frederick JR, Yang EC, Muenzer JR, Marotta NA, Berry MF, Atluri P, Woo YJ, Myocardial tissue elastic properties determined by

atomic force microscopy following SDF-1α angiogenic therapy for acute myocardial infarction. J. Thorac. Cardiovasc. Surg 143, 962–966 (2012). [PubMed: 22264415]

24. Dobson LE, Fairbairn TA, Musa TA, Uddin A, Mundie CA, Swoboda PP, Ripley DP, McDiarmid AK, Erhayiem B, Garg P, Malkin CJ, Blackman DJ, Sharples LD, Plein S, Greenwood JP, Sex-related differences in left ventricular remodeling in severe aortic stenosis and reverse remodeling after aortic valve replacement: A cardiovascular magnetic resonance study. Am. Heart J 175, 101–111 (2016). [PubMed: 27179729]

25. Williams M, Kodali SK, Hahn RT, Humphries KH, Nkomo VT, Cohen DJ, Douglas PS, Mack M, McAndrew TC, Svensson L, Thourani VH, Tuzcu EM, Weissman NJ, Kirtane AJ, Leon MB, Sex-related differences in outcomes after transcatheter or surgical aortic valve replacement in patients with severe aortic stenosis: Insights from the PARTNER Trial (Placement of Aortic Transcatheter Valve). J. Am. Coll. Cardiol 63, 1522–1528 (2014). [PubMed: 24561149]

26. Yahagi K, Torii S, Ladich E, Kutys R, Romero ME, Mori H, Kolodgie FD, Popma JJ, Virmani R, Finn AV, Pathology of self-expanding transcatheter aortic valves: Findings from the CoreValve US pivotal trials. Catheter. Cardiovasc. Interv 91, 947–955 (2018). [PubMed: 28895294]

27. Inohara T, Manandhar P, Kosinski AS, Matsouaka RA, Kohsaka S, Mentz RJ, Thourani VH, Carroll JD, Kirtane AJ, Bavaria JE, Cohen DJ, Kiefer TL, Gaca JG, Kapadia SR, Peterson ED, Vemulapalli S, Association of renin-angiotensin inhibitor treatment with mortality and heart failure readmission in patients with transcatheter aortic valve replacement. JAMA 320, 2231–2241 (2018). [PubMed: 30512100]

28. Dumonteil N, Vaccaro A, Despas F, Labrunee M, Marcheix B, Lambert E, Esler M, Carrie D, Senard JM, Galinier M, Pathak A, Transcatheter aortic valve implantation reduces sympathetic activity and normalizes arterial spontaneous baroreflex in patients with aortic stenosis. JACC Cardiovasc. Interv 6, 1195–1202 (2013). [PubMed: 24139928]

29. Gold L, Ayers D, Bertino J, Bock C, Bock A, Brody EN, Carter J, Dalby AB, Eaton BE, Fitzwater T, Flather D, Forbes A, Foreman T, Fowler C, Gawande B, Goss M, Gunn M, Gupta S, Halladay D, Heil J, Heilig J, Hicke B, Husar G, Janjic N, Jarvis T, Jennings S, Katilius E, Keeney TR, Kim N, Koch TH, Kraemer S, Kroiss L, Le N, Levine D, Lindsey W, Lollo B, Mayfield W, Mehan M, Mehler R, Nelson SK, Nelson M, Nieuwlandt D, Nikrad M, Ochsner U, Ostroff RM, Otis M, Parker T, Pietrasiewicz S, Resnicow DI, Rohloff J, Sanders G, Sattin S, Schneider D, Singer B, Stanton M, Sterkel A, Stewart A, Stratford S, Vaught JD, Vrkljan M, Walker JJ, Watrobka M, Waugh S, Weiss A, Wilcox SK, Wolfson A, Wolk SK, Zhang C, Zichi D, Aptamer-based multiplexed proteomic technology for biomarker discovery. PLOS ONE 5, e15004 (2010). [PubMed: 21165148]

30. Distler JHW, Schett G, Gay S, Distler O, The controversial role of tumor necrosis factor α in fibrotic diseases. Arthritis Rheum 58, 2228–2235 (2008). [PubMed: 18668576]

31. Borthwick LA, The IL-1 cytokine family and its role in inflammation and fibrosis in the lung. Semin. Immunopathol 38, 517–534 (2016). [PubMed: 27001429]

32. Goldberg MT, Han Y-P, Yan C, Shaw MC, Garner WL, TNF-α suppresses α-smooth muscle actin expression in human dermal fibroblasts: An implication for abnormal wound healing. J. Invest. Dermatol 127, 2645–2655 (2007). [PubMed: 17554369]

33. Kouba DJ, Chung K-Y, Nishiyama T, Vindevoghel L, Kon A, Klement JF, Uitto J, Mauviel A, Nuclear factor-κB mediates TNF-α inhibitory effect on α2(I) collagen (COL1A2) gene transcription in human dermal fibroblasts. J. Immunol 162, 4226–4234 (1999). [PubMed: 10201951]

34. Verrecchia F, Pessah M, Atfi A, Mauviel A, Tumor necrosis factor-α inhibits transforming growth factor-β/Smad signaling in human dermal fibroblasts via AP-1 activation. J. Biol. Chem 275, 30226–30231 (2000). [PubMed: 10903323]

35. Sexton TR, Wallace EL, Chen A, Charnigo RJ, Reda HK, Ziada KM, Gurley JC, Smyth SS, Thromboinflammatory response and predictors of outcomes in patients undergoing transcatheter aortic valve replacement. J. Thromb. Thrombolysis 41, 384–393 (2016). [PubMed: 26743061]

36. Brønnum H, Eskildsen T, Andersen DC, Schneider M, Sheikh SP, IL-1β suppresses TGF-β-mediated myofibroblast differentiation in cardiac fibroblasts. Growth Factors 31, 81–89 (2013). [PubMed: 23734837]

37. Li G, Qiao W, Zhang W, Li F, Shi J, Dong N, The shift of macrophages toward M1 phenotype promotes aortic valvular calcification. J. Thorac. Cardiovasc. Surg 153, 1318–1327.e1 (2017). [PubMed: 28283241]

38. Yu Z, Seya K, Daitoku K, Motomura S, Fukuda I, Furukawa K.-i., Tumor necrosis factor-α accelerates the calcification of human aortic valve interstitial cells obtained from patients with calcific aortic valve stenosis via the BMP2-Dlx5 pathway. J. Pharmacol. Exp. Ther 337, 16–23 (2011). [PubMed: 21205918]

39. Hjortnaes J, Goettsch C, Hutcheson JD, Camci-Unal G, Lax L, Scherer K, Body S, Schoen FJ, Kluin J, Khademhosseini A, Aikawa E, Simulation of early calcific aortic valve disease in a 3D platform: A role for myofibroblast differentiation. J. Mol. Cell. Cardiol 94, 13–20 (2016). [PubMed: 26996755]

40. Lim J, Ehsanipour A, Hsu JJ, Lu J, Pedego T, Wu A, Walthers CM, Demer LL, Seidlits SK, Tintut Y, Inflammation drives retraction, stiffening, and nodule formation via cytoskeletal machinery in a three-dimensional culture model of aortic stenosis. Am. J. Pathol 186, 2378–2389 (2016). [PubMed: 27392969]

41. Isoda K, Matsuki T, Kondo H, Iwakura Y, Ohsuzu F, Deficiency of interleukin-1 receptor antagonist induces aortic valve disease in BALB/c mice. Arterioscler. Thromb. Vasc. Biol 30, 708–715 (2010). [PubMed: 20110570]

42. Pislaru SV, Nkomo VT, Sandhu GS, Assessment of prosthetic valve function after TAVR. JACC Cardiovasc. Imaging 9, 193–206 (2016). [PubMed: 26846938]

43. Salinas P, Moreno R, Calvo L, Sánchez-Recalde A, Jiménez-Valero S, Galeote G, López-Fernández T, Ramírez U, Riera L, Plaza I, Moreno I, Mesa JM, López-Sendón JL, Long-term follow-up after transcatheter aortic valve implantation for severe aortic stenosis. Rev. Esp. Cardiol. (Engl. Ed.) 69, 37–44 (2016). [PubMed: 26234997]

44. Siwik DA, Chang DL-F, Colucci WS, Interleukin-1β and tumor necrosis factor-α decrease collagen synthesis and increase matrix metalloproteinase activity in cardiac fibroblasts in vitro. Circ. Res 86, 1259–1265 (2000). [PubMed: 10864917]

45. Zhang X, Xu B, Puperi DS, Yonezawa AL, Wu Y, Tseng H, Cuchiara ML, West JL, Grande-Allen KJ, Integrating valve-inspired design features into poly(ethylene glycol) hydrogel scaffolds for heart valve tissue engineering. Acta Biomater 14, 11–21 (2015). [PubMed: 25433168]

46. Wu Y, Puperi DS, Grande-Allen KJ, West JL, Ascorbic acid promotes extracellular matrix deposition while preserving valve interstitial cell quiescence within 3D hydrogel scaffolds. J. Tissue Eng. Regen. Med 11, 1963–1973 (2017). [PubMed: 26631842]

47. Duan B, Yin Z, Kang LH, Magin RL, Butcher JT, Active tissue stiffness modulation controls valve interstitial cell phenotype and osteogenic potential in 3D culture. Acta Biomater 36, 42–54 (2016). [PubMed: 26947381]

48. Grim JC, Brown TE, Aguado BA, Chapnick DA, Viert AL, Liu X, Anseth KS, A reversible and repeatable thiol–ene bioconjugation for dynamic patterning of signaling proteins in hydrogels. ACS Cent. Sci 4, 909–916 (2018). [PubMed: 30062120]

49. Aguado BA, Wu JJ, Azarin SM, Nanavati D, Rao SS, Bushnell GG, Medicherla CB, Shea LD, Secretome identification of immune cell factors mediating metastatic cell homing. Sci. Rep 5, 17566 (2015). [PubMed: 26634905]

50. Schlotter F, Halu A, Goto S, Blaser MC, Body SC, Lee LH, Higashi H, DeLaughter DM, Hutcheson JD, Vyas P, Pham T, Rogers MA, Sharma A, Seidman CE, Loscalzo J, Seidman JG, Aikawa M, Singh SA, Aikawa E, Spatiotemporal multi-omics mapping generates a molecular atlas of the aortic valve and reveals networks driving disease. Circulation 138, 377–393 (2018). [PubMed: 29588317]

51. Aguado BA, Hartfield RM, Bushnell GG, Decker JT, Azarin SM, Nanavati D, Schipma MJ, Rao SS, Oakes RS, Zhang Y, Jeruss JS, Shea LD, Biomaterial scaffolds as pre-metastatic niche mimics systemically alter the primary tumor and tumor microenvironment. Adv. Healthc. Mater 7, e1700903 (2018). [PubMed: 29521008]

52. Li L, Fan D, Wang C, Wang J-Y, Cui X-B, Wu D, Zhou Y, Wu L-L, Angiotensin II increases periostin expression via Ras/p38 MAPK/CREB and ERK1/2/TGF-β1 pathways in cardiac fibroblasts. Cardiovasc. Res 91, 80–89 (2011). [PubMed: 21367774]

53. Sato M, Shegogue D, Gore EA, Smith EA, Mcdermott PJ, Trojanowska M, Role of p38 MAPK in transforming growth factor β stimulation of collagen production by scleroderma and healthy dermal fibroblasts. J. Invest. Dermatol 118, 704–711 (2002). [PubMed: 11918720]

54. Voloshenyuk TG, Landesman ES, Khoutorova E, Hart AD, Gardner JD, Induction of cardiac fibroblast lysyl oxidase by TGF-β1 requires PI3K/Akt, Smad3, and MAPK signaling. Cytokine 55, 90–97 (2011). [PubMed: 21498085]

55. Molkentin JD, Bugg D, Ghearing N, Dorn LE, Kim P, Sargent MA, Gunaje J, Otsu K, Davis J, Fibroblast-specific genetic manipulation of p38 mitogen-activated protein kinase in vivo reveals its central regulatory role in fibrosis. Circulation 136, 549–561 (2017). [PubMed: 28356446]

56. Nagy E, Lei Y, Martínez-Martínez E, Body SC, Schlotter F, Creager M, Assmann A, Khabbaz K, Libby P, Hansson GK, Aikawa E, Interferon-γ released by activated CD8+ T lymphocytes impairs the calcium resorption potential of osteoclasts in calcified human aortic valves. Am. J. Pathol 187, 1413–1425 (2017). [PubMed: 28431214]

57. Nagy E, Andersson DC, Caidahl K, Eriksson MJ, Eriksson P, Franco-Cereceda A, Hansson GK, Bäck M, Upregulation of the 5-lipoxygenase pathway in human aortic valves correlates with severity of stenosis and leads to leukotriene-induced effects on valvular myofibroblasts 123, 1316–1325 (2011).

58. Aguado BA, Grim JC, Rosales AM, Watson-Capps JJ, Anseth KS, Engineering precision biomaterials for personalized medicine. Sci. Transl. Med 10, eaam8645 (2018).

59. Borer JS, Sharma A, Drug therapy for heart valve diseases. Circulation 132, 1038–1045 (2015). [PubMed: 26371236]

60. McCoy CM, Nicholas DQ, Masters KS, Sex-related differences in gene expression by porcine aortic valvular interstitial cells. PLOS ONE 7, e39980 (2012). [PubMed: 22808080]

61. Porras AM, McCoy CM, Masters KS, Calcific aortic valve disease: A battle of the sexes. Circ. Res 120, 604–606 (2017). [PubMed: 28209788]

62. Sritharen Y, Enriquez-Sarano M, Schaff HV, Casaclang-Verzosa G, Miller JD, Pathophysiology of aortic valve stenosis: Is it both fibrocalcific and sex specific? Physiology (Bethesda) 32, 182–196 (2017). [PubMed: 28404735]

63. Zusterzeel R, Mishra NK, Beydoun H, Laschinger J, Wu C, Dong LM, Lin J-A, Marinac-Dabic D, Strauss DG, Caños DA, Sex-specific outcomes after transcatheter aortic valve replacement: FDA patient-level meta-analysis of premarket clinical trials. J. Womens Health (Larchmt) 27, 808–814 (2018). [PubMed: 29741978]

64. Kodali S, Williams MR, Doshi D, Hahn RT, Humphries KH, Nkomo VT, Cohen DJ, Douglas PS, Mack M, Xu K, Svensson L, Thourani VH, Tuzcu EM, Weissman NJ, Leon M, Kirtane AJ, Sex-specific differences at presentation and outcomes among patients undergoing transcatheter aortic valve replacement: A cohort study. Ann. Intern. Med 164, 377–384 (2016). [PubMed: 26903039]

65. Thaden JJ, Nkomo VT, Suri RM, Maleszewski JJ, Soderberg DJ, Clavel M-A, Pislaru SV, Malouf JF, Foley TA, Oh JK, Miller JD, Edwards WD, Enriquez-Sarano M, Sex-related differences in calcific aortic stenosis: Correlating clinical and echocardiographic characteristics and computed tomography aortic valve calcium score to excised aortic valve weight. Eur. Heart J 37, 693–699 (2015). [PubMed: 26508159]

66. Villari B, Campbell SE, Schneider J, Vassalli G, Chiariello M, Hess OM, Sex-dependent differences in left ventricular function and structure in chronic pressure overload. Eur. Heart J 16, 1410–1419 (1995). [PubMed: 8746910]

67. Dobson LE, Fairbairn TA, Plein S, Greenwood JP, Sex differences in aortic stenosis and outcome following surgical and transcatheter aortic valve replacement. J. Womens Health (Larchmt) 24, 986–995 (2015). [PubMed: 26653869]

68. Ngo D, Sinha S, Shen D, Kuhn EW, Keyes MJ, Shi X, Benson MD, O'Sullivan JF, Keshishian H, Farrell LA, Fifer MA, Vasan RS, Sabatine MS, Larson MG, Carr SA, Wang TJ, Gerszten RE, Aptamer-based proteomic profiling reveals novel candidate biomarkers and pathways in cardiovascular disease. Circulation 134, 270–285 (2016). [PubMed: 27444932]

69. Liao Y, Smyth GK, Shi W, featureCounts: An efficient general purpose program for assigning sequence reads to genomic features. Bioinformatics 30, 923–930 (2014). [PubMed: 24227677]

70. Metsalu T, Vilo J, ClustVis: A web tool for visualizing clustering of multivariate data using principal component analysis and heatmap. Nucleic Acids Res 43, W566–W570 (2015). [PubMed: 25969447]

71. Pertea M, Kim D, Pertea GM, Leek JT, Salzberg SL, Transcript-level expression analysis of RNA-seq experiments with HISAT, StringTie and Ballgown. Nat. Protoc 11, 1650–1667 (2016). [PubMed: 27560171]

72. Yu G, Wang L-G, Han Y, He Q-Y, clusterProfiler: An R package for comparing biological themes among gene clusters. OMICS 16, 284–287 (2012). [PubMed: 22455463]

73. Genin M, Clement F, Fattaccioli A, Raes M, Michiels C, M1 and M2 macrophages derived from THP-1 cells differentially modulate the response of cancer cells to etoposide. BMC Cancer 15, 577 (2015). [PubMed: 26253167]
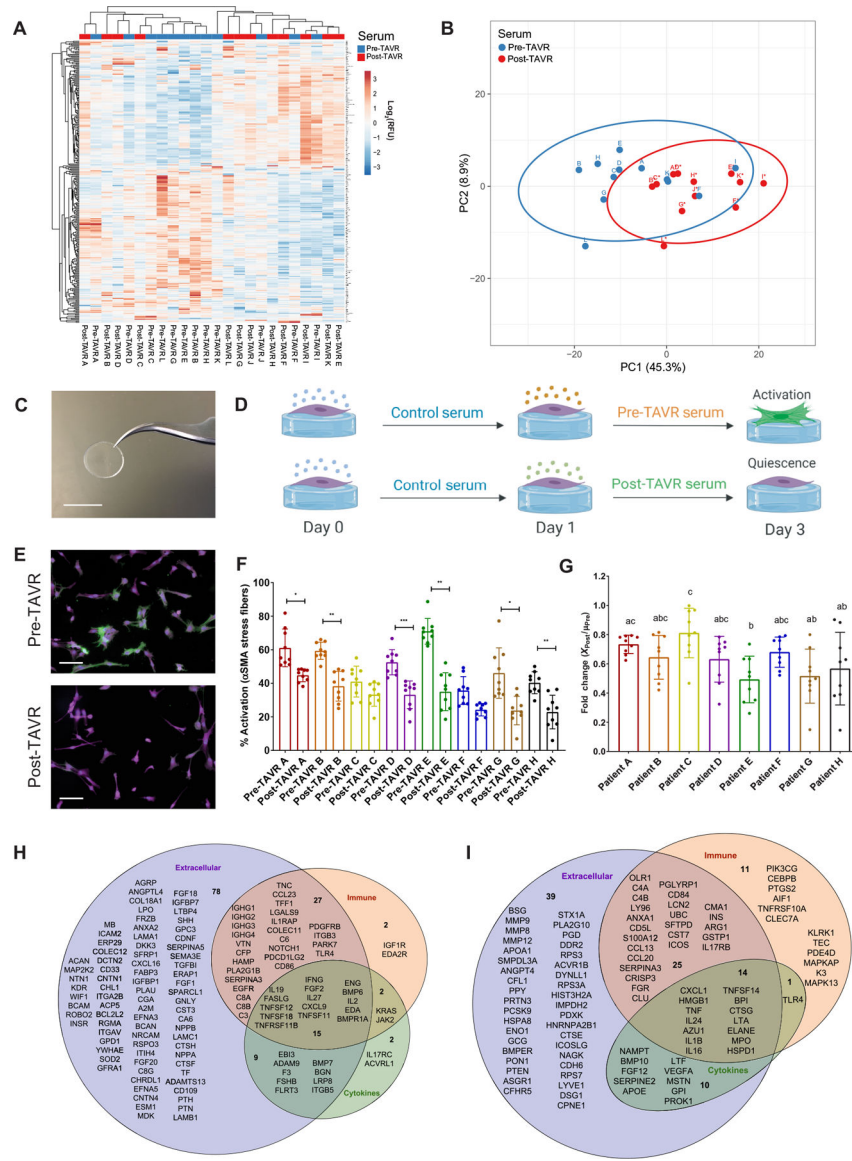
Fig. 1. Pre-TAVR serum activates VICs to a myofibroblast state, whereas post-TAVR serum mediates fibroblast quiescence.

(**A**) SOMAscan DNA aptamer array heatmap of individual $\log_2$-RFU values representing relative abundances for 283 significantly altered human serum proteins before and after a TAVR procedure ($n = 12$ pre-TAVR samples and $n = 12$ post-TAVR samples, paired t test, FDR-adjusted $P < 0.05$). (**B**) PCA plot of pre-TAVR and post-TAVR serum samples. (**C**) Photograph of a PEG hydrogel on a 12-mm-diameter glass coverslip. Scale bar, 12 mm. (**D**) Schematic of in vitro experiments using pre-TAVR and post-TAVR sera to treat porcine VICs on soft hydrogels (created with BioRender). (**E**) Representative images of VICs treated with pre- and post-TAVR serum. Green, α-SMA; magenta, cytoplasm; blue, nuclei. Scale bars, 100 μm. (**F**) Percentage of activated VICs treated with sera from TAVR patients ($n = 9$ measurements per group, one-way ANOVA with Tukey posttests, means ± SD shown, *$P < 0.05$, **$P < 0.01$, ***$P < 0.001$). (**G**) Fold change reduction of VIC activation in post-TAVR serum (X_{Post} values) normalized to the mean activation in pre-TAVR serum from the same

patient (μ_{Pre}). Groups with different letters indicate statistical significance ($n = 9$ measurements per group, one-way ANOVA with Tukey posttests, means ± SD shown, $P < 0.05$). (**H**) Pre-TAVR and (**I**) post-TAVR ontological categorization of serum proteins to identify factors contributing to myofibroblast activation and quiescence, respectively.
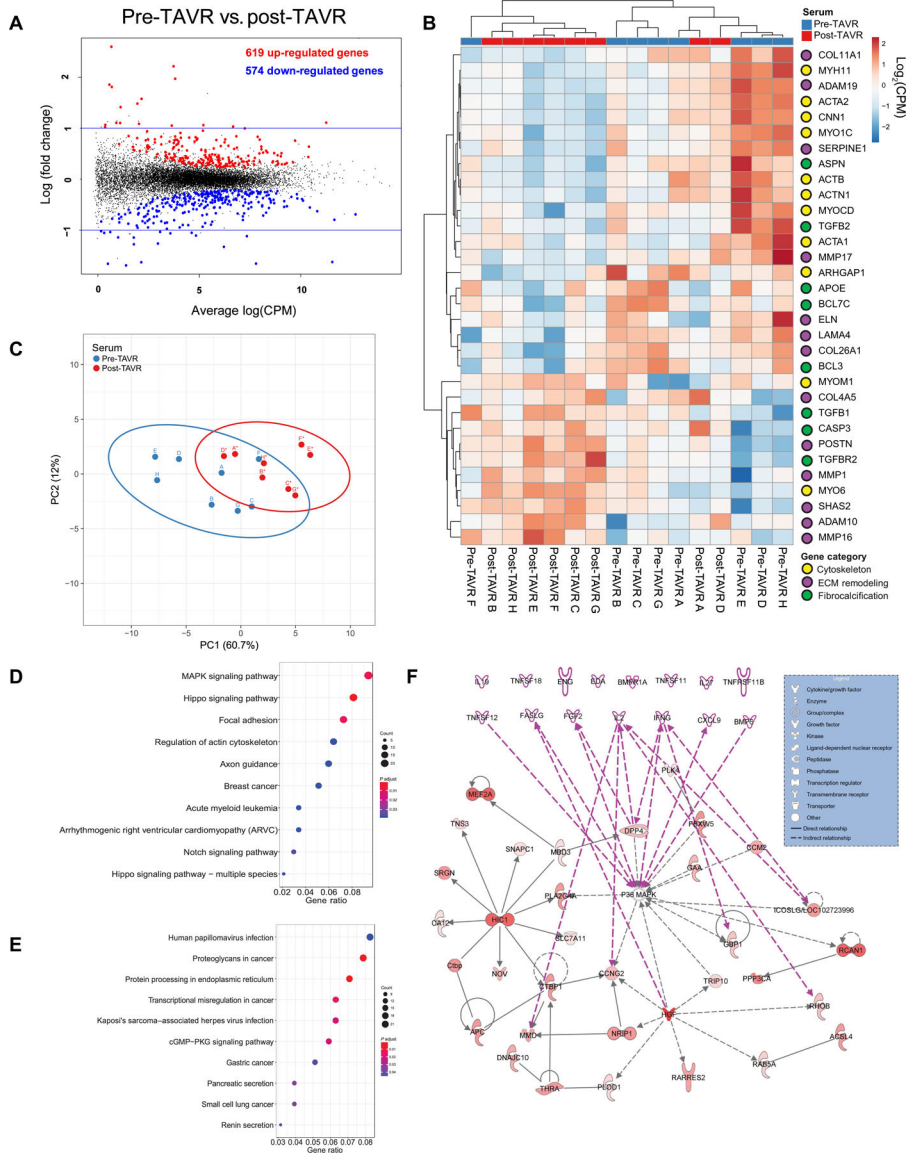
Fig. 2. Transcriptomics analysis reveals p38 MAPK signaling activity in pre-TAVR–mediated myofibroblast activation.

(**A**) MD plot reveals differentially expressed genes in porcine VICs treated with pre-TAVR and post-TAVR sera ($n = 8$ patients, quantile-adjusted conditional maximum likelihood method in edgeR, FDR-adjusted $P < 0.05$). (**B**) Log$_2$-transformed counts per million (CPM) values for key myofibroblast-associated genes ($n = 8$, all pre-TAVR versus post-TAVR comparisons, FDR-adjusted $P < 0.05$) and organized into cytoskeleton, ECM remodeling, and fibrocalcification categories. (**C**) PCA plot of key myofibroblast-associated genes. (**D** and **E**) Enriched KEGG signaling pathways for (D) up-regulated and (E) down-regulated genes in pre-TAVR serum relative to post-TAVR serum. (**F**) Ingenuity Pathway Analysis. Pre-TAVR serum protein candidates are represented by pink nodes and arrows among up-regulated genes.
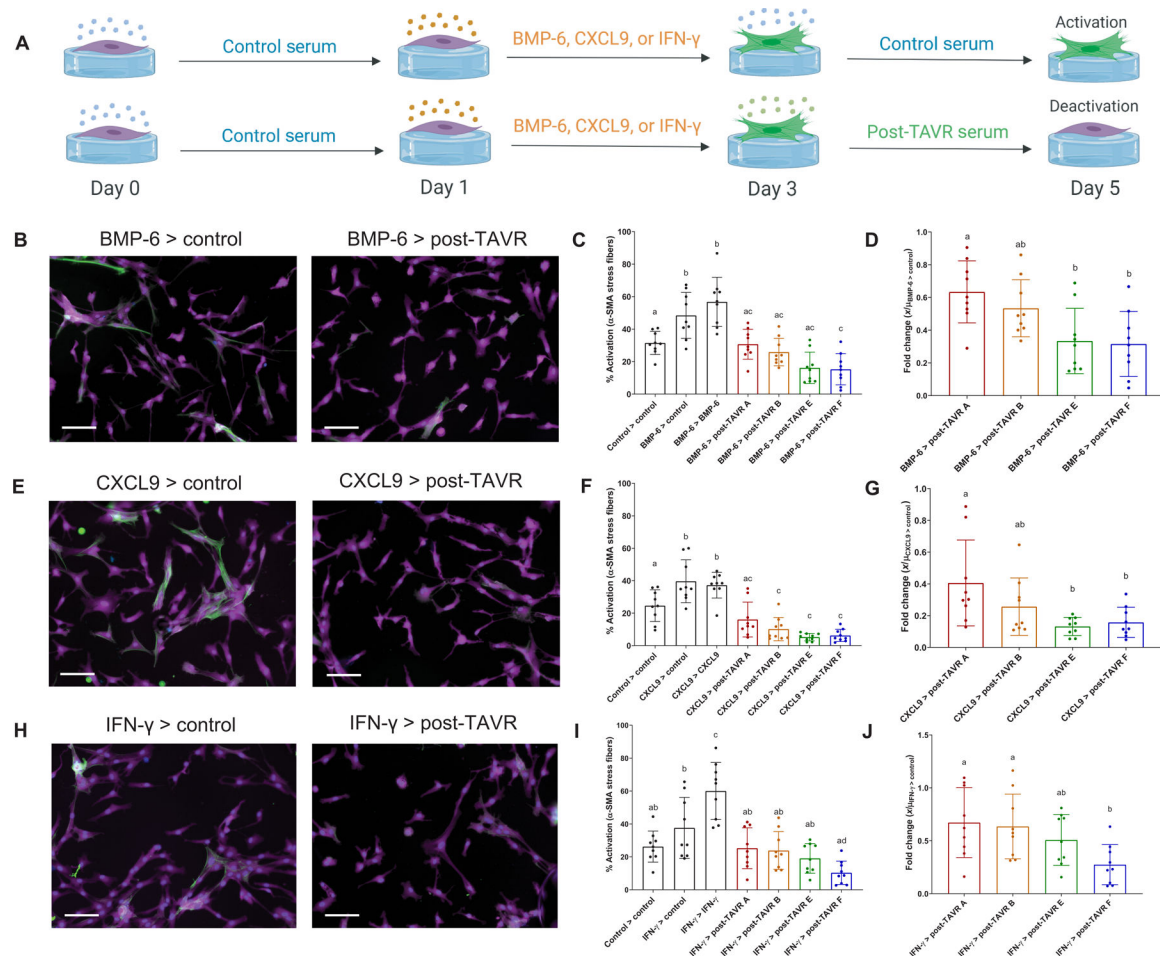
Fig. 3. Pre-TAVR serum factors (BMP-6, CXCL9, and IFN-γ) mediate myofibroblast activation.
(**A**) Schematic of valvular activation experiments with BMP-6, CXCL9, and IFN-γ (created with BioRender). Representative images of porcine VICs treated initially with (**B**) BMP-6, (**E**) CXCL9, or (**H**) IFN-γ for 2 days (left column) and then treated with either control media or post-TAVR serum (right column). Stains: green, α-SMA; magenta, cytoplasm; blue, nuclei. Scale bars, 100 μm. Percentage of activated VICs initially treated with (**C**) BMP-6, (**F**) CXCL9, or (**I**) IFN-γ and deactivated with post-TAVR serum from four patients. Patient-specific fold changes in post-TAVR deactivation in VICs initially activated with (**D**) BMP-6, (**G**) CXCL9, or (**J**) IFN-γ. Groups with different letters indicate statistical significance ($n = 9$ measurements per group, means ± SD shown, one-way ANOVA with Tukey posttests, $P < 0.05$).
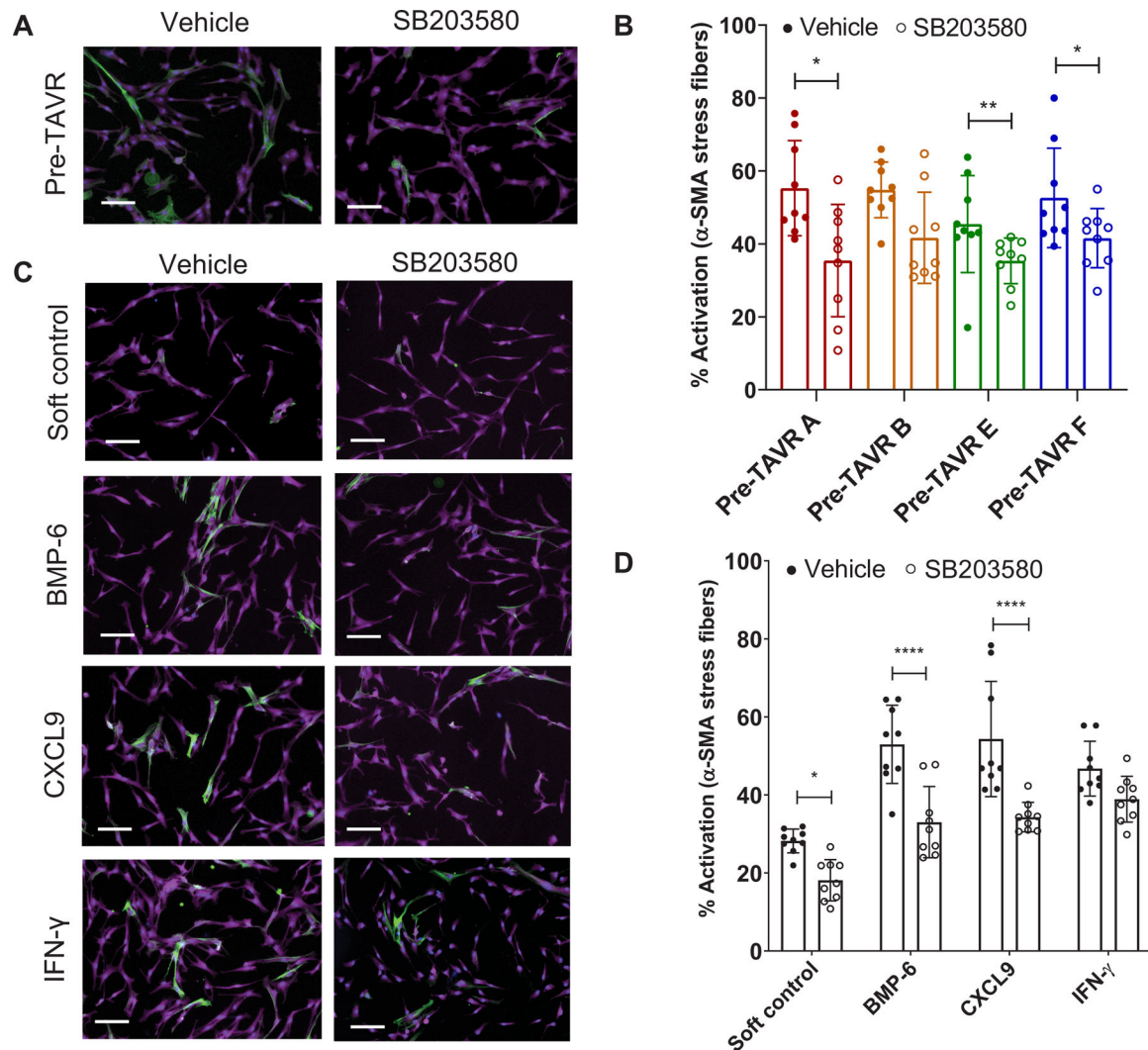
Fig. 4. Validation of p38 MAPK signaling in mediating myofibroblast activation on soft hydrogels in the presence of various factors.
(**A**) Representative images of porcine VICs treated with pre-TAVR serum in the absence or presence of 20 μM SB203580. Stains: green, α-SMA; magenta, cytoplasm; blue, nuclei. Scale bars, 100 μm. (**B**) VIC activation in pre-TAVR serum ($n = 4$ patients) in the absence or presence of SB203580 ($n = 9$ measurements per group, means ± SD shown, unpaired t test for each patient, $*P < 0.05$, $**P < 0.01$). (**C**) Representative images of VICs treated with BMP-6, CXCL9, and IFN-γ in the absence or presence of 20 μM SB203580. Stains: green, α-SMA; magenta, cytoplasm; blue, nuclei. Scale bars, 100 μm. (**D**) VIC activation in BMP-6, CXCL9, and IFN-γ in the absence or presence of SB203580 ($n = 9$ measurements per group, means ± SD shown, two-way ANOVA with Tukey posttests, $*P < 0.05$, $****P < 0.001$).
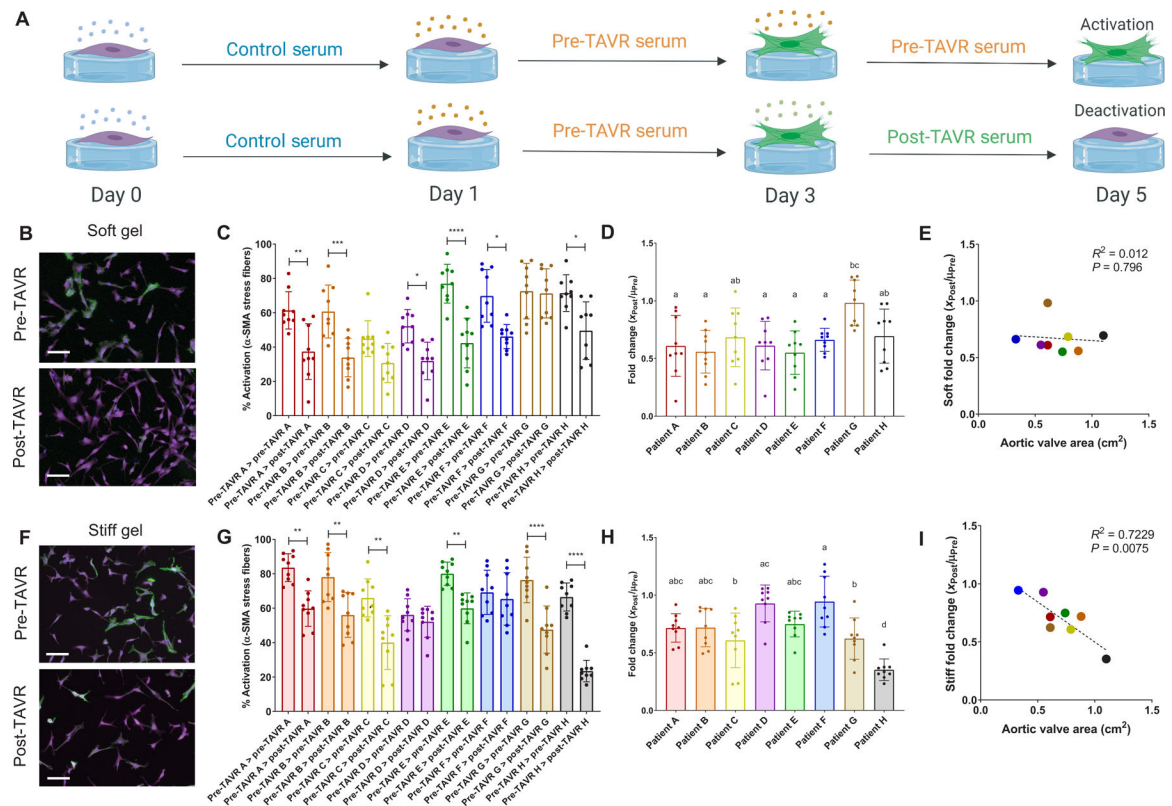
Fig. 5. Post-TAVR serum deactivates valvular myofibroblasts activated with pre-TAVR serum on soft and stiff hydrogels.

(**A**) Schematic of myofibroblast deactivation experiments (created with BioRender). (**B**) Representative images and (**C**) percentage of activated porcine VICs on soft hydrogels treated initially with pre-TAVR serum and subsequently with either pre-TAVR or post-TAVR serum. (**D**) Fold change of VIC deactivation on soft hydrogels in post-TAVR serum (X_{Post} values) normalized to the mean activation in pre-TAVR serum from the same patient (μ_{Pre}). (**E**) Scatter plot of fold change in VIC deactivation on soft hydrogels versus aortic valve area measurements. (**F**) Representative images and (**G**) percentage of activated VICs on stiff hydrogels treated initially with pre-TAVR serum and subsequently with either pre-TAVR or post-TAVR serum. (**H**) Fold change of VIC deactivation on stiff hydrogels in post-TAVR serum (X_{Post} values) normalized to the mean activation in pre-TAVR serum from the same patient (μ_{Pre}). (**I**) Scatter plot of fold change in VIC deactivation on stiff hydrogels versus aortic valve area measurements. Stained images: green, α-SMA; magenta, cytoplasm; blue, nuclei. Scale bars, 100 μm. For all bar graphs, $n = 9$ measurements per group, means ± SD shown, and significance tested with one-way ANOVA for all data and indicated as *$P <$ 0.05, **$P <$ 0.01, ***$P <$ 0.001, ****$P <$ 0.0001, or groups with different letters indicate statistical significance ($P <$ 0.05).
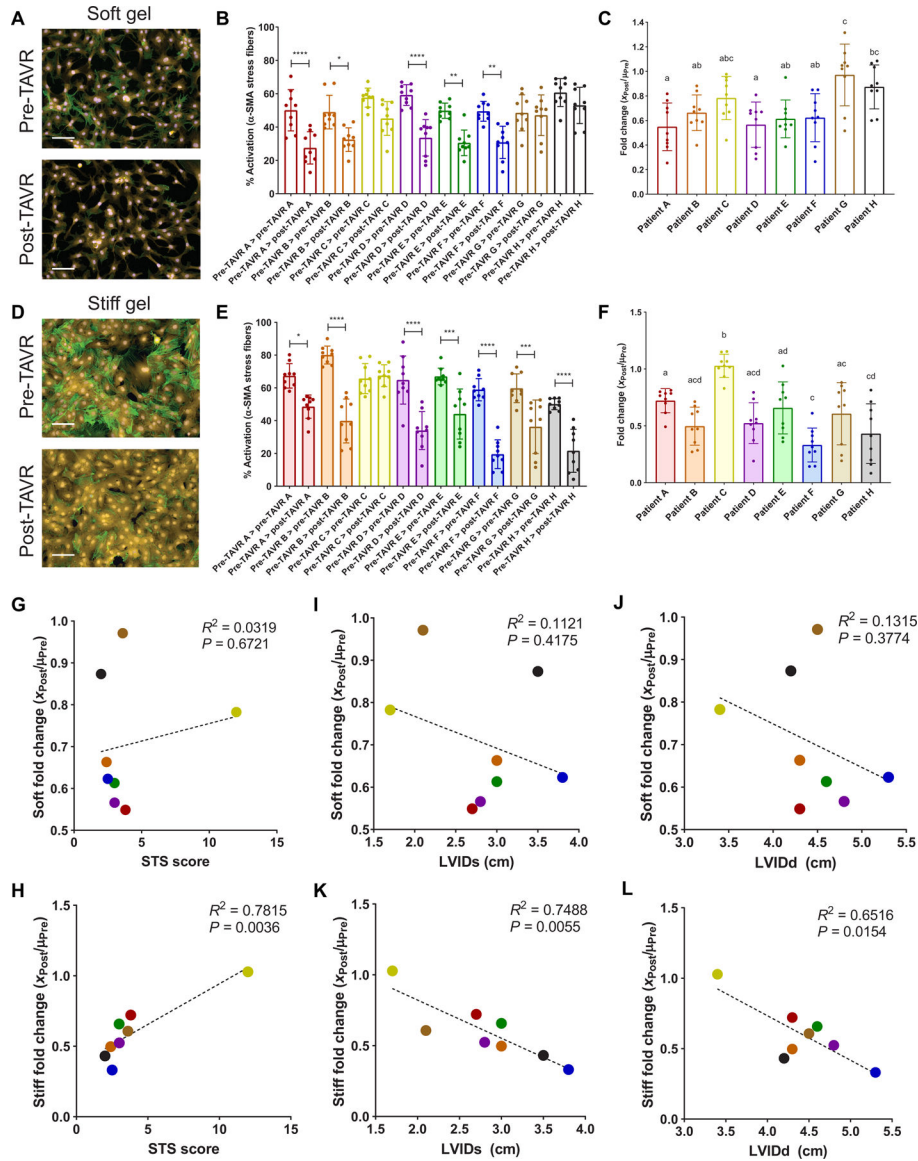
Fig. 6. Post-TAVR serum deactivates cardiac myofibroblasts activated with pre-TAVR serum on soft and stiff hydrogels.

(**A**) Representative images and (**B**) percentage of activated ARVFs on soft hydrogels treated initially with pre-TAVR serum and subsequently with either pre-TAVR or post-TAVR serum. (**C**) Fold change of ARVF deactivation on soft hydrogels in post-TAVR serum (X_{Post} values) normalized to the mean activation in pre-TAVR serum from the same patient (μ_{Pre}). (**D**) Representative images and (**E**) percentage of activated ARVFs on stiff hydrogels treated initially with pre-TAVR serum and subsequently with either pre-TAVR or post-TAVR serum. (**F**) Fold change of ARVF deactivation on stiff hydrogels in post-TAVR serum (X_{Post} values) normalized to the mean activation in pre-TAVR serum from the same patient (μ_{Pre}). (**G** and **H**) Scatter plots of fold change in ARVF deactivation on (G) soft and (H) stiff hydrogels versus patient STS scores. (**I** and **J**) Scatter plots of patient fold change in ARVF deactivation on soft hydrogels versus (I) LVIDs and (J) LVIDd measurements. (**K** and **L**) Scatter plots of fold change in ARVF deactivation on stiff hydrogels versus patient (K)

LVIDs and (L) LVIDd measurements. Stained images: green, α-SMA; yellow, cytoplasm; blue, nuclei. Scale bars, 100 μm. For all bar graphs, $n = 9$ measurements per group, means ± SD shown, and significance tested with one-way ANOVA for all data and indicated as *$P <$ 0.05, **$P < 0.01$, ***$P < 0.001$, ****$P < 0.0001$, or groups with different letters indicate statistical significance ($P < 0.05$).
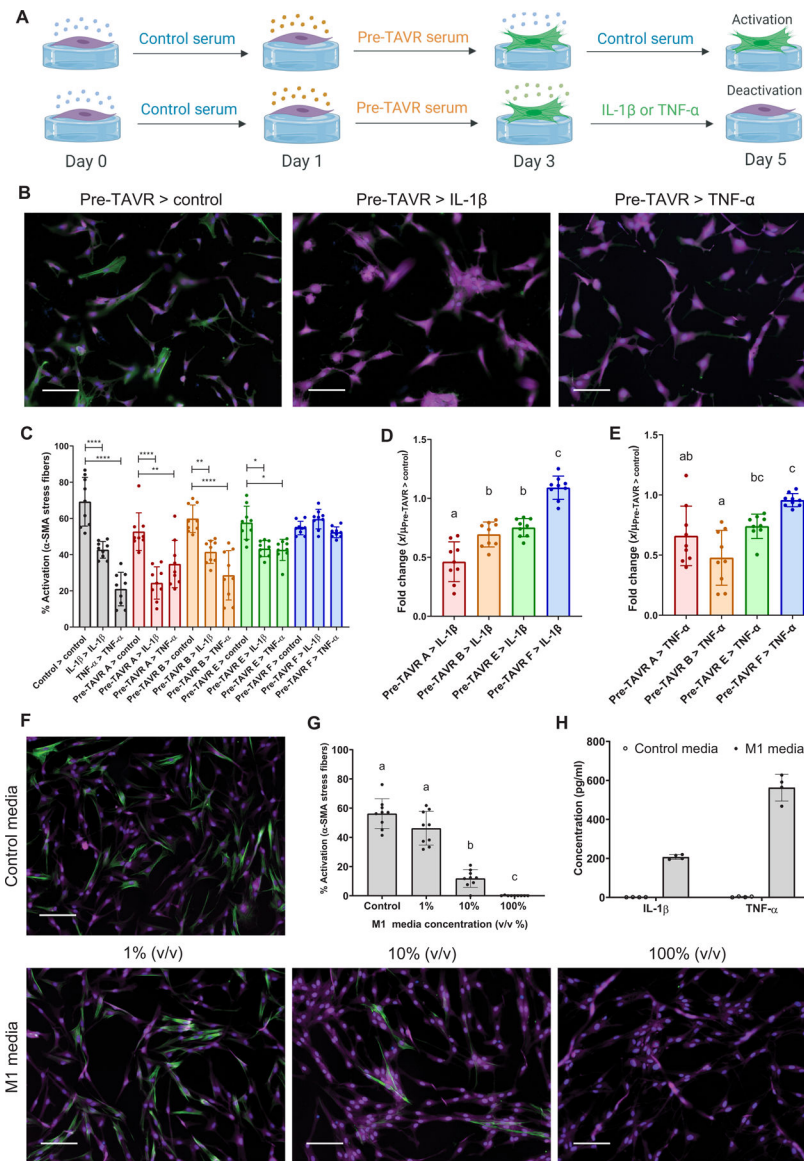
Fig. 7. Inflammatory macrophage factors identified in post-TAVR serum mediate myofibroblast deactivation on stiff hydrogels.

(**A**) Schematic of myofibroblast deactivation experiments with IL-1β or TNF-α (created with BioRender). (**B**) Representative images and (**C**) percentage of activated porcine VICs treated with pre-TAVR serum ($n = 4$ different patients), followed by treatments with control media, IL-1β (10 ng/ml), or TNF-α (10 ng/ml). (**D** and **E**) Patient-specific fold changes in (D) IL-1β– or (E) TNF-α–mediated deactivation in VICs initially activated with pre-TAVR serum ($n = 4$ patients). (**F**) Representative images and (**G**) percentage of activated VICs treated with proinflammatory M1 macrophage conditioned media at varying dilutions. (**H**) IL-1β and TNF-α concentrations in control and M1 macrophage conditioned media measured with ELISA. Stained images: green, α-SMA; magenta, cytoplasm; blue, nuclei. Scale bars, 100 μm. For all bar graphs, $n = 9$ measurements per group, means ± SD shown, and significance tested with one-way ANOVA for all data and indicated as *$P < 0.05$, **$P <$

0.01, ****$P < 0.0001$, or groups with different letters indicate statistical significance ($P < 0.05$).
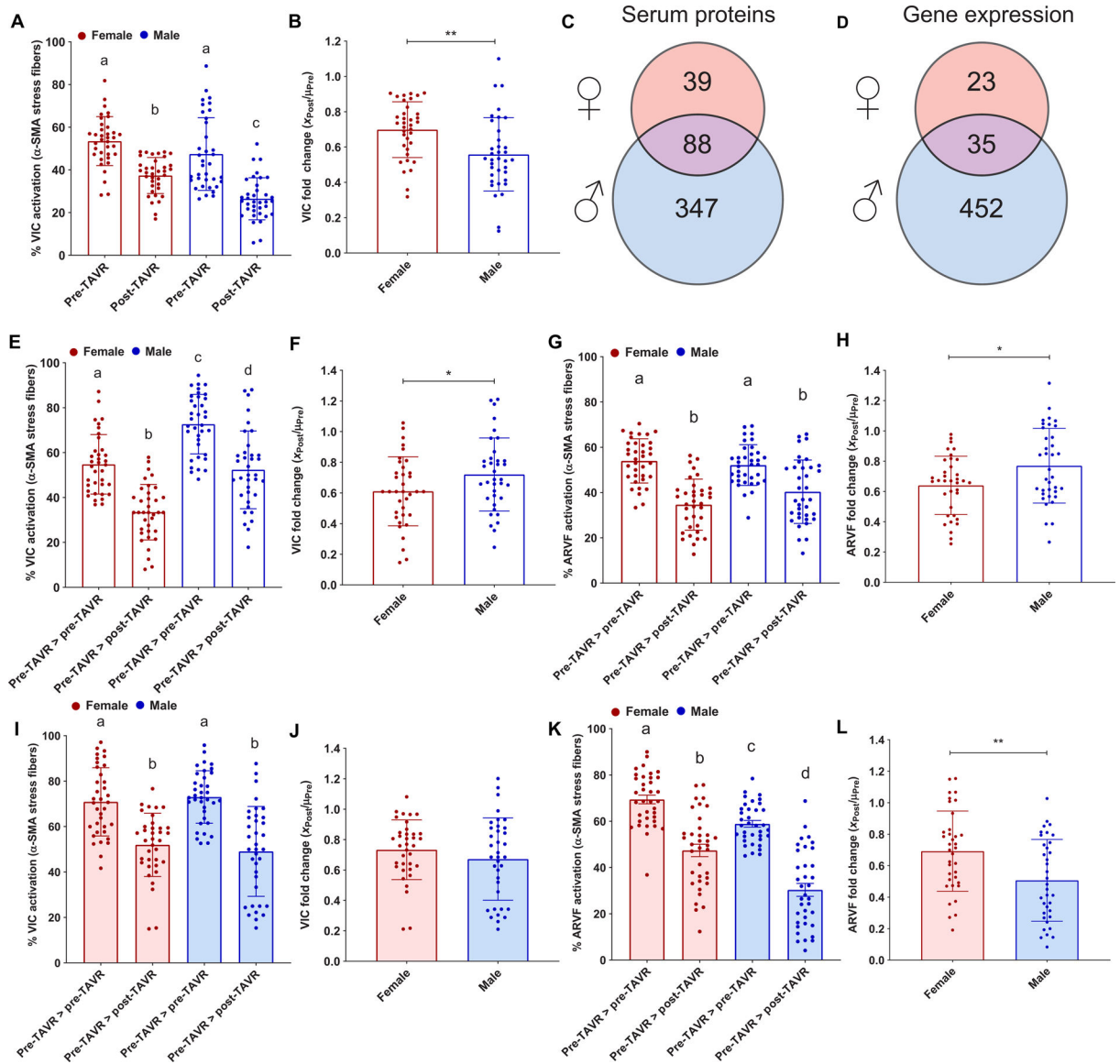
Fig. 8. VIC and ARVF response to pre-TAVR and post-TAVR sera from male and female patients with AVS.
(**A**) Porcine VIC activation on soft hydrogels in the presence of female and male pre-TAVR and post-TAVR sera. (**B**) Fold change of VIC activation on soft hydrogels in post-TAVR serum (X_{Post} values) normalized to the mean activation in pre-TAVR serum from female and male patients (μ_{Pre}). (**C**) Total number of differentially abundant proteins in pre-TAVR serum relative to post-TAVR serum for male and female patients (paired t test, $P < 0.05$). (**D**) Total number of differentially expressed genes in VICs treated with pre-TAVR serum relative to post-TAVR serum from male and female patients (quantile-adjusted conditional maximum likelihood method in edgeR, FDR-adjusted $P < 0.05$). (**E**) VIC deactivation and (**F**) deactivation fold change on soft hydrogels in the presence of female and male post-TAVR serum. (**G**) ARVF deactivation and (**H**) deactivation fold change on soft hydrogels in the presence of female and male post-TAVR serum. (**I**) VIC deactivation and (**J**) deactivation fold change on stiff hydrogels in the presence of female and male post-TAVR serum. (**K**)

ARVF deactivation and (**L**) deactivation fold change on stiff hydrogels in the presence of female and male post-TAVR serum. For all bar graphs, $n = 36$ measurements were pooled together per group, means ± SD shown, with significance tested using unpaired t tests or one-way ANOVA and indicated as *$P < 0.05$ and **$P < 0.01$.